

<https://helda.helsinki.fi>

CIP2A Interacts with TopBP1 and Drives Basal-Like Breast Cancer Tumorigenesis

Laine, Anni

2021-08

Laine , A , Nagelli , S G , Farrington , C , Butt , U , Cvrljevic , A N , Vainonen , J P , Feringa , F M , Gronroos , T J , Gautam , P , Khan , S , Sihto , H , Qiao , X , Pavic , K , Connolly , D C , Kronqvist , P , Elo , L L , Maurer , J , Wennerberg , K , Medema , R H , Joensuu , H , Peuhu , E , de Visser , K , Narla , G & Westermarck , J 2021 , ' CIP2A Interacts with TopBP1 and Drives Basal-Like Breast Cancer Tumorigenesis ' , Cancer Research , vol. 81 , no. 16 , pp. 4319-4331 . <https://doi.org/10.1158/0008-5472.CAN-20-3651>

<http://hdl.handle.net/10138/335008>

<https://doi.org/10.1158/0008-5472.CAN-20-3651>

acceptedVersion

Downloaded from Helda, University of Helsinki institutional repository.

This is an electronic reprint of the original article.

This reprint may differ from the original in pagination and typographic detail.

Please cite the original version.

1 CIP2A interacts with TopBP1 and drives basal-like breast 2 cancer tumorigenesis

3 Anni Laine^{1,2*}, Srikar G. Nagelli^{1,3*}, Caroline Farrington^{4,5}, Umar Butt^{1,3}, Anna N. Cvrljevic¹,
 4 Julia P. Vainonen¹, Femke M. Feringa^{6#}, Tove J. Grönroos^{7,8}, Prson Gautam⁹, Sofia
 5 Khan¹, Harri Sihto¹⁰, Xi Qiao¹, Karolina Pavic¹, Denise C. Connolly¹¹, Pauliina Kronqvist³,
 6 Laura L. Elo^{1,3}, Jochen Maurer¹², Krister Wennerberg⁹, Rene H. Medema⁶, Heikki
 7 Joensuu¹⁰, Emilia Peuhu^{1,3}, Karin de Visser^{2,13}, Goutham Narla^{4,5}, and Jukka
 8 Westermarck^{1,3§}

10 ¹Turku Bioscience Centre, University of Turku and Åbo Akademi University, Turku, Finland

11 ²Division of Tumor Biology & Immunology, Oncode Institute, The Netherlands Cancer
 12 Institute, Amsterdam, The Netherlands

13 ³Institute of Biomedicine, University of Turku, Turku, Finland

14 ⁴Division of Genetic Medicine, Department of Internal Medicine, University of Michigan,
 15 Ann Arbor, MI, 48105, USA.

16 ⁵Rogel Cancer Center, University of Michigan, Ann Arbor, MI, 48109, USA.

17 ⁶Division of Cell Biology, Oncode Institute, The Netherlands Cancer Institute, Amsterdam,
 18 The Netherlands

19 ⁷Turku PET Centre, University of Turku, Turku, Finland

20 ⁸Department of Oncology and Radiotherapy, Turku University Hospital, Turku, Finland

21 ⁹Institute for Molecular Medicine Finland (FIMM), HiLIFE, University of Helsinki, Helsinki,
 22 Finland

23 ¹⁰Department of Pathology, University of Helsinki, Helsinki University Hospital, Helsinki,
 24 Finland

25 ¹¹Molecular Therapeutics Program, Fox Chase Cancer Center, Philadelphia, PA, USA

26 ¹²Department of Obstetrics and Gynecology, University Hospital Aachen (UKA), 52074
 27 Aachen, Germany

28 ¹³Department of Immunohematology and Blood Transfusion, Leiden University Medical
 29 Centre, Leiden, The Netherlands

30
 31 *These authors contributed equally

32 #Current address: Department of Molecular and Cellular Neurobiology, Faculty of Science,
 33 Center for Neurogenomics and Cognitive Research, Amsterdam Neuroscience, Vrije
 34 Universiteit Amsterdam, 1081HV, Amsterdam, The Netherlands

38 **Running title:** CIP2A drives basal-like breast cancers via TopBP1 and MYC

41 § **Corresponding author:** Jukka Westermarck, Turku Bioscience Centre, University of
42 Turku, Tykistökatu 6B, 20540 Turku, Finland, tel: +358-294502880, fax: +358-294505040,
43 e-mail: jukwes@utu.fi

44

45 **Conflicts of interest:** The authors declare no potential conflicts of interest

46

47 **Total word count:** 7495, 7 figures

48

49

50

Abstract

Basal-like breast cancers (BLBC) are characterized by defects in homologous recombination (HR), deficient mitotic checkpoint, and high proliferation activity. Here, we discover CIP2A as a candidate driver of BLBC. CIP2A was essential for DNA-damage-induced initiation of mouse BLBC-like mammary tumors and for survival of homologous recombination defective (HRD) BLBC cells. CIP2A was dispensable for normal mammary gland development and for unperturbed mitosis, but selectively essential for mitotic progression of DNA-damaged cells. A direct interaction between CIP2A and a DNA repair scaffold protein TopBP1 was identified and CIP2A inhibition resulted in enhanced DNA damage-induced TopBP1 and RAD51 recruitment to chromatin in mammary epithelial cells. In addition to its role in tumor initiation, and survival of BRCA-deficient cells, CIP2A also drove proliferative MYC and E2F1 signaling in basal-like triple negative breast cancer (BL-TNBC) cells. Clinically, high CIP2A expression was associated with poor patient prognosis in BL-TNBCs but not in other breast cancer subtypes. Small molecule reactivators of PP2A (SMAPs) inhibited CIP2A transcription, phenocopied the CIP2A-deficient DNA damage response (DDR), and inhibit growth of patient-derived BLBC xenograft. In summary, these results demonstrate that CIP2A directly interacts with TopBP1 and coordinates DNA-damage induced mitotic checkpoint and proliferation, thereby driving BLBC initiation and progression. SMAPs could serve as a surrogate therapeutic strategy to inhibit the oncogenic activity of CIP2A in BLBCs.

Significance: These results identify CIP2A as a non-genetic driver and therapeutic target in basal-like breast cancer that regulates DNA-damage-induced G2/M checkpoint and proliferative signaling.

Keywords: ATR, RHNO1, Nibrin, Double stranded DNA break, DT-061

76 **Introduction**

77

78 One of the most aggressive and clinically challenging breast cancer subtypes is the basal-
 79 like breast cancer (BLBC)(1-3). Based on transcriptional signatures of the breast cancer
 80 subtypes (4), the hallmarks of BLBCs are high proliferation activity, G2/M checkpoint
 81 dysregulation, ATR/BRCA pathway activity, and high DNA replication. Additionally,
 82 molecular characteristics of BLBCs include high genetic instability, BRCA mutations, TP53
 83 inactivation, and dysregulation of EGFR (1-4). About 75% of BLBCs belong to the triple-
 84 negative breast cancer subtype (BL-TNBCs), devoid of ER, PR and HER2 (1). In addition
 85 to their frequently aggressive clinical appearance, the lack of these targetable receptors
 86 makes BLBCs therapeutically very challenging. Despite the near saturated genetic
 87 knowledge of breast cancer, like some other subtypes as well, no clear genetic oncogenic
 88 drivers have been identified for the BLBCs (1,3).

89

90 Among the breast cancer subtypes, BLBCs have the highest mutational burden as a result
 91 of acquisition of BRCA mutations, or other defects in the homologous recombination (HR)
 92 pathways (1-4). Normal HR proficient cells respond to double stranded DNA breaks (DSB)
 93 by activating the G2/M cell cycle checkpoint resulting in mitotic arrest (5). To allow mitotic
 94 progression under DNA damaging conditions, transformed cells instead have developed
 95 strategy to dampen G2/M checkpoint signaling (5,6). Based on the high mutational burden
 96 observed in BLBC, it could be hypothesized that a potential BLBC driver mechanism has
 97 the ability to coordinately dampen the DNA-damage induced G2/M checkpoint, and to
 98 support high proliferation activity in premalignant mammary epithelial cells. One of the
 99 DDR proteins involved in G2/M checkpoint signaling is DNA Topoisomerase II binding
 100 protein 1 (TopBP1)(7), which is a scaffold protein that interacts with the checkpoint kinase

101 ATR (8). In the presence of DSBs, TopBP1 promotes RAD51 chromatin loading resulting
 102 in G2/M arrest (9-12). RAD51 foci formation has been associated in BLBCs as a marker of
 103 BRCA deficiency and HR impairment (4,13). These features make TopBP1-mediated
 104 RAD51 regulation a candidate G2/M checkpoint mechanism in BLBC (5,7,10).

105

106 Recently the serine/threonine phosphatase PP2A has gained attention as a druggable
 107 tumor suppressor (14-16). Of specific relevance to this work, is the role of serine/threonine
 108 phosphatases in the DNA damage response at chromatin (6), which could link them to
 109 cancer types with homologous recombination defects, and high mutational burden, such
 110 as BLBCs. PP2A is inhibited in most cancers by non-genetic mechanisms including high
 111 expression of endogenous inhibitor proteins such as CIP2A, PME-1 or SET, or changes in
 112 carboxymethylation to the C terminal tail of the catalytic domain (15,17). *CIP2A* is
 113 expressed at low levels in normal mammary gland tissue (18). However, *CIP2A*
 114 transcription is induced by *TP53* mutation via increased E2F1 activity (18,19), and by
 115 EGFR pathway activation (20,21), features closely linked to BLBC (1). However, it is
 116 currently unclear what role CIP2A plays in BLBC initiation, or progression. Notably,
 117 understanding of CIP2A-related cancer initiation mechanisms is also therapeutically
 118 relevant due to the recent development of small molecule activators of the CIP2A-inhibited
 119 PP2A-B56 heterotrimer that demonstrate potent antitumor activities (14,16).

120

121 In this study, we provide the first evidence for an essential role for CIP2A in tumor initiation
 122 in cancer. Specifically, we demonstrate by using both chemical and transgenic tumor
 123 models that CIP2A is essential for the initiation of mouse BLBC tumors, but not for the
 124 initiation of skin, ovarian, lung or stomach tumors. Furthermore, among transformed breast
 125 cancer cell types, CIP2A is essential for survival of BRCA/TP53-mutant BLBC cells.

126 Mechanistically, the role for CIP2A in driving BLBC initiation and progression can be
127 explained by its capacity to coordinately regulate key BLBC hallmarks; specifically the
128 G2/M checkpoint and cellular proliferation. Molecularly we discover direct CIP2A
129 interaction with TopBP1 and provide evidence for CIP2A-mediated inhibition of both
130 TopBP1 and RAD51 recruitment to chromatin upon DNA-damage in premalignant
131 mammary epithelial cells. CIP2A also promotes pro-proliferative MYC and E2F1 activities
132 in BLBC cells. Finally, we discover that small molecules shown previously to activate
133 PP2A (16,22), transcriptionally inhibit *CIP2A* expression, and serve as candidate
134 therapeutics for CIP2A-positive BLBCs.

135

136

137 **Materials and Methods**

138

139 Mouse experiments

140 All animal work protocols were approved either by the Project Authorisation Board of the
 141 Regional State Administrative Agency for Southern Finland, the Animal Ethics Committee
 142 of the Netherlands Cancer Institute or the Institutional Animal Care and Use Committee at
 143 the Case Western Reserve University, which is certified by the American Association of
 144 Accreditation for Laboratory Animal Care under protocol # 2013-0132.

145

146 For DMBA-induced tumors in *WT* and *Cip2a*^{-/-} female mice, several independent cohorts
 147 of the mice were administered with 1mg of DMBA dissolved in 200μl of corn oil by oral
 148 gavage once a week for 6 weeks starting at 12-14 weeks of age as previously described
 149 (23). The mice were monitored twice a week for tumor formation until morbidity. Mice were
 150 sacrificed upon tumor burden and/or when they showed general signs of illness. For
 151 DMBA-induced mutation load and *Cip2a* mRNA expression in *WT* and *Cip2a*^{-/-}
 152 premalignant mammary gland tissues, the mice were sacrificed 2 weeks after the last
 153 DMBA treatment. DMBA/TPA protocol for skin tumorigenesis and experiments with *Cip2a*^{-/-}
 154 mice crossed with an ovarian cancer mouse model *TgMISIIR-Tag* are described in
 155 supplementary materials and methods. Tissue samples collected for extraction of RNA
 156 and genomic DNA were snap frozen into liquid nitrogen. Tissue samples for histochemical
 157 and for immunohistochemical analysis were fixed in formalin.

158

159 Mouse tumor cell lines were generated from spontaneous mammary tumors of following
 160 breast cancer mouse models: *K14Cre; Brca1*^{F/F}; *Trp53*^{F/F}(*KB1P*) (24), *K14Cre; Cdh1*^{F/F};
 161 *Trp53*^{F/F}(*KEP*) (25) and *Wap-cre; Cdh1*^{F/F}; *Akt1*^{E17K}(*WEA*) (26). Tumor cell lines were

generated by collecting tumors in cold PBS and minced by chopping with scalpels. Aggregates were plated out. *KEP* and *WEA* tumor cell line cultures were incubated at 37°C with 5% CO₂ and 20% O₂. *KB1P* cell lines were incubated at 37°C with 5% CO₂ and 3% O₂. Homogenous epithelial cell morphology was obtained after cultures were passaged 2-3 times. Used cell culture media are described in Table S1.

Analysis of human breast cancer patient sample cohorts

FinHer study (HUCH 426/E6/00) was approved by an ethics committee of the Helsinki University Central Hospital (Helsinki, Finland). Study participants provided written informed consent before study entry. The study was conducted in accordance of the Declaration of Helsinki. The role of *CIP2A* in disease-free survival of breast cancer patients in the GSE21653 cohort was analyzed by using an online platform 'R2: Genomics Analysis and Visualization Platform' (<https://hgserver1.amc.nl/cgi-bin/r2/main.cgi>). More detailed description of analysis of both cohorts can be found from supplemental data.

Cell culture and transfections

All the commercial cell lines used in this paper were purchased from American Type Culture Collection (ATCC) or Leibniz Institute's German Collection of Microorganisms and Cell Cultures (DSMZ). All the cells in culture were negative on periodically testing for mycoplasma using Mycoplasma Detection Kit (Roche). All the human and mouse cells, their culture conditions and supplements used for cell culture are listed in Table S1. Breast cancer stem-like cells (BCSCs) were isolated from TNBC patients who received standard chemotherapy and cultured as described previously (27).

Antibodies, RNAs, primers, DNA constructs and drugs.

187 Antibodies (along with dilutions for each application), plasmids and sequences of siRNAs,
188 gRNAs and primers used are listed in Table S2. All chemical inhibitors and drugs used are
189 listed in the Table S3.

190

191 Mitotic index experiments

192 Mitotic index experiments were conducted by modifying previously published protocol
193 described in (7). Briefly, MCF10A cells were transfected with indicated siRNAs for 24
194 hours, following which they were seeded into ibidi 8 well μ slides (ibiTreat #80826) for 24
195 hours. Cells were irradiated with 10Gy radiation followed by Nocodazole block (100ng/ml),
196 one hour after IR for 18 hours. After the indicated time points, cells were stained for
197 phospho-Histone H3 (Ser10) using similar immunofluorescence protocols as mentioned
198 above. Images were taken on Zeiss Axiovert or EVOS fl Microscope with 10X objective
199 and quantified using ImageJ software (RRID:SCR_003070). Experiment was repeated 3
200 times.

201

202 **Results**

203 ***Cip2a* is selectively required for initiation of DMBA-induced mammary tumors in** 204 **mice**

205 To address whether CIP2A is truly essential for the initiation of cancer *in vivo*, we
 206 challenged several independent cohorts of the previously described *Cip2a*^{-/-} mice (19,28)
 207 with a chemical carcinogenesis protocol consisting of six consecutive doses of the
 208 genotoxic agent 7,12-dimethylbenz[a]anthracene (DMBA) (Fig. 1A). Similar to other
 209 polyaromatic hydrocarbons, DMBA forms covalent DNA adducts, and induces a DNA
 210 damage response (DDR) including activation of γH2AX, ATR, and RAD51 (29). Oral
 211 exposure of mice to DMBA induces mouse BLBCs (23), but also several other cancers,
 212 allowing us to assess the relative importance of *Cip2a* to tumor development across
 213 different cancer types. As compared to a model combining DMBA and
 214 medroxyprogesterone acetate (MPA), the DMBA-only mammary tumors are initiated with
 215 much longer latency (23). Importantly, the tumor initiating cell type of mammary tumors
 216 induced by DMBA-only is basaloid cells, and molecularly these tumors faithfully resemble
 217 human BLBCs (23).

218
 219 As expected (29), DMBA treatment induced a significant increase in the mutational load in
 220 non-tumorigenic mammary gland tissue as soon as only 2 weeks after the last DMBA
 221 dose; however the mutational load (Fig. 1 B and Table S4), or overall survival (Fig. S1A)
 222 was not associated with the *Cip2a* genotype. When assessed by palpation, external
 223 observation, and by tissue pathology analysis upon autopsy of the mice with any
 224 symptoms of reduced well-being, tumors in five different tissue types were observed in the
 225 DMBA-treated mice (Fig. 1C). Notably, while incidence of tumors in ovary, lung, skin or

stomach were not altered in *Cip2a*^{-/-} mice, mammary tumors showed almost absolute dependence on *Cip2a* for tumor initiation (Fig. 1C, D and S1B).

To control for the possibility that lack of genotype dependence of other cancer types on *Cip2a* was a result of leakage of the genetrap cassette used for *Cip2a* gene silencing (28), we confirmed the absence of CIP2A protein expression in ovarian cancer tissues from *Cip2a*^{-/-} mice (Fig. S1C). We further confirmed that *Cip2a* was dispensable for skin and ovarian tumorigenesis by independent *in vivo* models. To this end, we crossed *Cip2a*^{-/-} mice with the MISIIR-Tag mouse model producing tumors resembling high grade ovarian cancer (30), and did not observe any notable difference in ovarian tumorigenesis between *Cip2a* wild-type (*WT*) or *Cip2a*^{-/-} mice by PET/CT-imaging or by visual inspection after autopsy (Fig. S1D,E). For the skin tumorigenesis model, we used a classical DMBA/TPA two-stage skin tumorigenesis protocol and again did not observe any differences in skin tumor initiation between the *Cip2a* genotypes (Fig. S1F).

Combined, these results in multiple independent *in vivo* models strongly suggest that CIP2A is required for the propagation of DNA-damaged mammary basaloid epithelial cells. To validate that this is a cell intrinsic property of CIP2A, we tested the impact of CIP2A silencing on mitotic progression of MCF-10A basal like immortalized mammary epithelial cells treated with ionizing radiation (IR). Notably, whereas inhibition of checkpoint kinase CHK1 abrogated the G2/M checkpoint and CIP2A silencing did not impact mitotic progression of untreated MCF-10A cells, CIP2A was found to be indispensable for G2/M progression in IR-treated MCF10A cells (Fig. 1E and S1G). To provide independent validation to these results, we surveyed results from a genetic screen in HAP1 cells (31) (see Fig. S1H for technical description). Directly supportive of the role for CIP2A in

allowing cell propagation under DNA damage, CIP2A was the only tested PP2A inhibitor protein that was essential under repeated low-dose irradiation (Fig. 1F).

These results establish essentiality for *Cip2a* for the initiation of DNA-damage induced mammary tumors previously confirmed to faithfully represent mouse BLBCs (23). As such the results represent the first evidence for a critical role for CIP2A in tumor initiation.

***Cip2a* is induced by DMBA in premalignant mammary gland tissue and drives initiation of mouse BLBC-like tumors**

A key criterion for a cancer driver candidate involved in tumor initiation, is expression in premalignant tissue prior tumorigenesis. Consistent with negligible CIP2A protein expression in normal human mammary glands (18), *Cip2a* mRNA was expressed at a very low level in *WT* mouse mammary glands (Fig. 2A). Importantly, non-tumorous *WT* mammary glands sampled 2 weeks after the last dose of DMBA (Fig. 1A) displayed significantly increased *Cip2a* mRNA expression (Fig. 2A). In line with a suggested role as a disease driver, *Cip2a* mRNA expression was induced significantly more in mammary tumors from DMBA-treated *WT* mice (Fig. 2A). However, as mammary tumors were induced in only some of the mammary glands in each of the DMBA-treated *WT* mice, we conclude that *Cip2a* expression is essential, but not sufficient alone to induce tumorigenesis.

Based upon the molecular characterization of the mammary tumors from DMBA-treated *WT* mice, the majority of the characterized tumors had BLBC or BL-TNBC phenotypes

(Fig. 2B,C and S2A). This is consistent with a previous report demonstrating that the tumor initiating cells from this DMBA model are of basaloid origin (23). The small number of estrogen receptor (ER) positive tumors observed is consistent with TCGA data that about 10% of human BLBCs are ER positive. Furthermore, although use of different DMBA *in vivo* protocol was recently shown to result in ER positive tumors (32), it was demonstrated by using the DMBA protocol used in our study that serial transplantation of ER positive tumors yielded ER negative secondary tumors, suggesting that ER expression was not a driver mechanism in these tumors (23). To study the impact of *Cip2a* on DMBA-induced mammary gland gene expression profiles, we performed RNA-sequencing analysis of non-tumorigenic mammary glands from mice housed for more than 4 months after the last dose of DMBA. Fully consistent with basaloid and HRD phenotype, *Cip2a* was found to control G2/M checkpoint, and proliferative signaling via the MYC and E2F1 pathways (Fig. 2D). The tumors in *WT* mice were also highly proliferative based on Ki67 staining, and displayed both CIP2A and MYC protein overexpression potentially indicative of their known feed-forward regulatory loop (33)(Fig. 2B). Evaluating the CIP2A positivity in DMBA-treated pre-tumorigenic mammary gland duct epithelial cells and from mammary tumors in *WT* mice, revealed predominantly cytoplasmic, but also nuclear CIP2A protein expression (Fig.S2B). This pattern is consistent with previous analysis indicating that there is a small pool of nuclear CIP2A in propagating cells (34), and indicate a potential function for nuclear CIP2A in early mammary tumorigenesis. Notably, the lack of predominantly BLBC tumors in *Cip2a*^{-/-} mice was not related to any genotype-associated alterations in the basal and luminal epithelial cell ratio in the mammary gland (Fig. S2C-F). Furthermore, we did not observe any notable differences in the mammary gland development and branching morphogenesis between *WT* and *Cip2a*^{-/-} mice (Fig. S2G).

298

299 Collectively, these results demonstrate that although *Cip2a* is dispensable for normal
 300 mouse mammary development, DMBA-elicited induction of *Cip2a* mRNA expression is
 301 required for initiation of mouse BLBC-like tumors.

302

303 **Co-dependence analysis reveals a functional association between CIP2A, TopBP1** 304 **and G2/M checkpoint regulation**

305

306 Although our results strongly indicate that the previously reported CIP2A-MYC feed-
 307 forward loop (33,35,36) is highly relevant for proliferation in DMBA-induced BLBCs (Fig.
 308 2B and S2A), MYC regulation is unlikely to explain either the newly discovered role for
 309 CIP2A in G2/M checkpoint regulation (Fig. 1E,F and S2A), or its essentiality for *in vivo*
 310 propagation of DNA-damaged mammary epithelial cells (Fig. 1C,D and S2G).
 311 Furthermore, as TPA/DMBA-induced skin tumorigenesis is dependent on MYC (37), but
 312 totally independent of CIP2A (Fig. S1F), we hypothesized that CIP2A is involved in the
 313 regulation of a yet uncharacterized MYC-independent, but HRD-related mechanism. To
 314 identify such mechanism in an unbiased manner, we surveyed a CRISPR/Cas9-based
 315 dropout screen repository from DepMap (Avana 2020 Q1; <https://depmap.org>), to identify
 316 genes that are most significantly similar in their essentiality with *CIP2A*.

317

318 Remarkably, across 739 human cancer cell lines all the top 10 co-dependent genes with
 319 *CIP2A* (i.e. functionally most similar to CIP2A) were DDR genes (Fig. 3A). Notably, out of
 320 these top ten *CIP2A*-associated DDR factors, *CIP2A* was at the genome-wide level the
 321 most significantly similar gene for *RHNO1*, *TOPBP1*, *POLQ*, *NBN* and *PARP1* (Fig. 3A). In
 322 the case of *TOPBP1*, the co-dependency with *CIP2A* was greater than with *ATR* (Fig. 3B),
 323 which is the bona-fide TopBP1 DDR effector (7,8). On the other hand, strongly supporting

the selectivity of CIP2A's association with DDR mechanisms, and arguing against MYC being the sole effector of CIP2A in tumorigenesis, there was no overlapping genes found among the top ten co-dependent genes between *CIP2A* and *MYC* (Fig. 3A and S3A).

When analyzed for functional protein association networks by STRING database (<https://string-db.org>), the top CIP2A-associated proteins (Fig. 3A) formed a tight protein network (Fig. 3C), that was functionally linked with HRD-associated processes such as "G2/M DNA damage checkpoint", "Homology directed Repair", and "Processing of DNA double-strand break ends" (Fig. 3D). Interestingly, in a recent PP2A-related phosphoproteome survey (38), CIP2A was found to prevent the dephosphorylation of Nibrin (NBN), which was one of the TopBP1 protein network members (Fig. 3C). NBN is known to co-operate with TopBP1 in ATR activation, and dephosphorylation of serine 432 of NBN, as observed in CIP2A depleted cells (Fig. S3B)(38), impairing cell survival under IR (39). CIP2A was also recently found to be a NBN co-dependent gene in PARP inhibitor treated cells (40).

Additional evidence for the intertwining of CIP2A with the TopBP1 complex was obtained by mRNA co-expression analysis across 1156 cell lines from the Broad institute Cancer Cell line Encyclopedia. Of the *CIP2A* co-dependent genes (Fig. 3A), *TOPBP1* and *POLQ* were also among the 25 most significantly co-expressed genes with CIP2A (Fig. 3E and Fig. S4A). Both *TOPBP1* and *POLQ* showed very significant co-expression with *CIP2A* also when only the BLBC cell lines were surveyed (Fig. S4B). The DepMap co-dependence data was also utilized to understand the interesting difference in CIP2A dependence in the initiation of mammary and ovarian cancers (Fig. 1). To this end, we analyzed in a pair-wise fashion the correlation between dependence on either *CIP2A*, or

one of the functionally most similar genes *RHNO1*, *TOPBP1*, *POLQ*, *NBN* and *PARP1* (rank 1 genes from Fig. 3A) across either BLBC or HGSOC cell lines. *TOPBP1* and *NBN* had higher co-dependence with CIP2A in BLBC than in HGSOC cells, while in HGSOC, *RHNO1* was more co-dependent with CIP2A (Fig. 3F). These differences may provide one plausible explanation for the differential requirement of *Cip2a* for DMBA-induced BLBC-like, but not ovarian cancer initiation (Fig. 1C, and S1B). Notably, *TOPBP1* did not show CIP2A co-dependence in HGSOC cells, but was co-dependent in BLBC cells (Fig. 3F).

CIP2A dampens TopBP1-RAD51 function under DNA damage

Although the results above identify a potential novel role for CIP2A in TopBP1-complex mediated G2/M arrest, there is currently no evidence for a direct mechanistic link between CIP2A and TopBP1. Here, by using a genome-wide Y2H assay with a human breast cancer cDNA library, TopBP1 was identified with very high confidence as an interaction partner for CIP2A (Fig. 4A) (Table S5). As Y2H assay only detects direct interactions between two proteins, we conclude that the CIP2A-TopBP1 association does not involve PP2A. However, as indicated by NBN phosphorylation data (38)(Fig. S3B), CIP2A may still protect proteins in the TopBP1 complex from PP2A-mediated dephosphorylation.

CIP2A is predominantly a cytoplasmic protein, but based on our current (Fig. S2B) and previous data (34), there is also a nuclear CIP2A pool in propagating cells *in vitro* and *in vivo*. Interaction between TopBP1 and endogenous nuclear CIP2A was confirmed from propagating cells by co-immunoprecipitation and proximity ligation analysis (Fig. 4B and S5A). γ H2AX also co-immunoprecipitated with TopBP1 and CIP2A from DNase treated cellular lysates indicating that direct TopBP1-CIP2A interaction occurs at chromatin (Fig.

374 4B). By narrowing down the minimal shared region between TopBP1 fragments interacting
 375 with CIP2A in the Y2H assay, the interaction with CIP2A was delineated to be mediated by
 376 the stretch of amino acids 829-853 located between 5th and 6th BRCT domain of TopBP1
 377 (Fig. 4A, Table S5). The region between the 5th and 6th BRCT domain was also essential
 378 for interaction by co-immunoprecipitation analysis (Fig. 4C,D). Notably, the interaction was
 379 greatly strengthened by the presence of the ATR-activation domain (AAD) of TopBP1
 380 adjacent to 6th BRCT repeat (Fig. 4C,D). As, no other DNA repair related proteins were
 381 identified in CIP2A Y2H screen (Table S5), the results support a model where direct
 382 binding to the scaffold protein TopBP1 mediates CIP2A interaction with the DDR network.
 383
 384 Directly linking CIP2A to TopBP1-regulated DDR, CIP2A inhibition significantly increased
 385 ATR phosphorylation in the propagating premalignant mammary cell line MCF-10A (Fig.
 386 4E), and the highest phosphorylation of the ATR target H2AX (γ H2AX)(41) was observed
 387 in CIP2A-depleted cells overexpressing AAD variant of TopBP1 (Fig. 4F). The role of
 388 CIP2A in dampening IR-induced γ H2AX was validated in primary mammary epithelial cells
 389 isolated from WT and *Cip2a*^{-/-} mice (Fig. S5B). Although PP2A has been validated as a
 390 γ H2AX phosphatase in replication stressed cells (42), we interpret that increased γ H2AX
 391 phosphorylation in CIP2A depleted replicating cells is rather due to increased TopBP1-
 392 associated ATR activity (7,8,41). Further supporting the role of CIP2A in dampening
 393 TopBP1 function, CIP2A depletion in IR-treated proliferating cells resulted in significantly
 394 enhanced chromatin recruitment of TopBP1 (Fig. 4G,H). This was specific to TopBP1, as
 395 CIP2A did not impact IR-induced p53BP1 chromatin recruitment (Fig. S5C). As CIP2A
 396 depletion did not induce ATM phosphorylation (Fig. S5D) which is a known mechanism
 397 increasing TopBP1 chromatin recruitment (8), we postulate that CIP2A prevents TopBP1
 398 chromatin binding by direct interaction with its BRCT-domains (Fig. 4A). In BRCA wild-type

cells TopBP1 mediates G2/M arrest in response to IR by promoting RAD51 chromatin loading (10-12,43). Consistent with the G2/M arrest phenotype (Fig. 1E and 2D), and increased TopBP1 foci formation (Fig. 4G,H), the *Cip2a*^{-/-} mammary epithelial cells exposed to IR displayed significantly enhanced RAD51 chromatin recruitment 2 hours after irradiation (Fig. 4I,J). Importantly, increased RAD51 retention at chromatin was observed still 6 hours after irradiation in *Cip2a*^{-/-} mammary epithelial cells, indicating for a long-term defect in DNA repair foci clearance (Fig. S5E).

Together with the established role for TopBP1/RAD51 complex in DNA damage-induced G2/M checkpoint activity (7,9-11,43), the discovered CIP2A-mediated inhibition of TopBP1 and RAD51 chromatin recruitment provides a mechanism for dampening of the G2/M checkpoint in CIP2A-positive premalignant mammary epithelial cells (Fig. 4K).

CIP2A is essential for survival of TP53/BRCA-mutant BLBC cells

Next, we assessed whether the role of CIP2A as a mouse BLBC driver candidate translates to human BLBC. Firstly, both *CIP2A* and *TOPBP1* mRNA was found to be highest expressed in BLBC across the human breast cancer subtypes (Fig. 5A and S6A,B). *TP53* mutations in BLBC may result in activation of *CIP2A* gene promoter activity through the p21-E2F1 pathway (19) and accordingly, a significant correlation between *TP53* mutation, and high *CIP2A* expression was confirmed in the GSE21653 cohort (Fig. S6C). The clinical relevance and selectivity of CIP2A for human BLBC was evident from patient survival analysis. Both high mRNA and protein expression of CIP2A predicted poor disease-free and overall survival only in BL-TNBC, but not in non-BL-TNBC breast cancers (Fig. 5B-E, and S6D-H). CIP2A neither had a predictive role among patients with ER-

424 positive tumors, or in unselected breast cancers (Fig. S6D,G). Notably, the 5-year survival
 425 of patients with highly CIP2A positive BL-TNBC tumor was only about 50% in both patient
 426 cohorts (Fig. 5B, D), indicating that these high CIP2A tumors are particularly aggressive.
 427 Furthermore, high CIP2A expression significantly associated with mutation load in TNBC
 428 tumors based on TCGA data (Fig. S6I). This finding indicates that while CIP2A expression
 429 is not impacting mutation frequency per se (Fig. 1B), it allows survival of DNA-damaged
 430 cells (Fig. 1F), and thereby accumulation of tumor mutational load in fully developed
 431 TNBCs.

432

433 To assess the BLBC cell dependence on *CIP2A*, we surveyed the Dep-Map essentiality
 434 database across 33 breast cancer cell lines. Among the 12 cell lines with CERES gene
 435 dependency score less than -0.4 for *CIP2A* loss, the great majority of cell lines were found
 436 to be BLBC cells (Fig. 5F, Table S6). Notably, all except one of these most *CIP2A*-
 437 dependent BLBC cells carried either a *BRCA1* or *BRCA2* mutation which is a hallmark of
 438 BLBCs (Fig. 5F). Furthermore, in a genetically defined CRISPR/Cas9 model, *Cip2a* was
 439 found to be essential for colony growth of mouse mammary tumor cells depleted for *Trp53*
 440 and *Brca1* (*KB1P*; basal-type)(24)(Fig. 5G). However, *Cip2a* was dispensable for growth of
 441 either *Trp53/E-cadherin* mutant mammary tumor cells (*KEP*; invasive lobular carcinoma-
 442 type)(25)(Fig. 5G), or cells from the mice with activated AKT and loss of E-cadherin in
 443 mammary tumor cells (*WEA*; invasive lobular carcinoma-type)(26)(Fig. S7A). Furthermore,
 444 RNA-sequencing analysis from the most *CIP2A*-dependent *TP53*-mutant BLBC cell line
 445 (Fig. 5H, S7B) and HCC38 (*TP53* mutant/*BRCA1* promoter methylation/*BRCA2* mutant),
 446 revealed that CIP2A drove similar BLBC and HRD-associated gene expression programs
 447 as was observed from DMBA-treated mouse mammary tissue (Fig. 2D and Fig. 5I). The
 448 role of CIP2A in inhibiting the dephosphorylation of the activating phosphorylation sites in

both MYC and E2F1 was confirmed by western blot analyses (Fig. 5J). Finally, consistent with recent identification of CIP2A as an essential gene in PARP inhibitor talazoparib-treated cells (40), CIP2A depletion hypersensitized BRCA-proficient MDA-MB-231 cells to two different PARP inhibitors (Fig. S7C).

These data reveal essentiality of CIP2A for the survival BRCA-deficient BLBC cells, and thus fully support the mouse data indicating the driver role of CIP2A in BLBC. Clinically the data introduces CIP2A as a potential biomarker to identify BL-TNBC patients with particularly aggressive disease.

Transcriptional CIP2A targeting by SMAPs as potential BLBC therapy

Effective treatment of BLBCs represents a significant unmet medical need. As our data indicate that CIP2A regulates PP2A activity towards both the TopBP1 complex (Fig. 3C and S3B), as well as towards MYC and E2F1 (Fig. 5J), we tested whether a recently developed series of Small Molecule Activators of PP2A (SMAPs) (14,16), could be used to target CIP2A-expressing BLBC. SMAPs activate the CIP2A-regulated PP2A-B56alpha heterotrimer (14,44), and the cellular effects of SMAPs in cancer cells are both correlated with PP2A reactivation capacity, and can be rescued by concomitant PP2A inhibition (22,45).

Treatment with two independent SMAPs (DBK-1154 and DT-061) resulted in a robust inhibition of cell viability in eight established BL-TNBC cell lines (Fig. 6A and S8A), and in five BLBC patient-derived cancer stem cell-like lines (27)(Fig. 6B). Notably, consistent with notion that these cell lines were derived from tumors of patients that had undergone neoadjuvant chemotherapy, these CIP2A positive (Fig. S8B) patient-derived BLBC cell

lines showed resistance to classical chemotherapies (Fig. 6B). Directly supportive of the therapeutic relevance of these observations, oral DT-061 therapy resulted in significant inhibition of tumor growth of an orthotopic PDX model from a patient with *TP53* mutant, EGFR+ BLBC over a 40-day treatment period (Fig. 6C). Similar to other *in vivo* studies with SMAPs (14,46,47), we did not observe any treatment-related adverse effects in mice. Importantly the control tumors were CIP2A positive, whereas tumors from DT-061 treated mice showed a clear trend for reduced CIP2A protein levels (Fig. S8C,D).

Related to a potential link between SMAP response and CIP2A, western blot analyses revealed a surprising inhibition of CIP2A protein expression by SMAPs at 24 hours (Fig. 6D,E and S8E-G). Indicative of transcriptional level regulation, CIP2A protein inhibition was accompanied with inhibition of *CIP2A* mRNA expression (Fig. 6F and S8G). The candidate mechanism for SMAP-elicited *CIP2A* inhibition was evaluated by studying the time course of CIP2A inhibition in relation to its two known upstream activators ERK and MYC (20,21,33), which both are inhibited by SMAPs (45). Whereas inhibition of ERK phosphorylation by SMAP preceded inhibition of CIP2A expression, MYC was inhibited in SMAP treated cells after CIP2A inhibition (Fig. 6G, and S8H).

SMAPs, representing surrogate CIP2A inhibitors, were next tested for possible effects on biomarkers of CIP2A activity. Consistent with results in CIP2A-depleted cells (Fig. 4), SMAPs induced potent checkpoint signaling exemplified by phosphorylation of H2AX, ATR and CHK2 (Fig. 6H,I and S9A,B). SMAP treatment for 24 hours also resulted in potent inhibition of MYC protein expression (Fig. S9C). Regarding causality between SMAP-induced checkpoint activation and CIP2A inhibition, SMAP-elicited CHK2 phosphorylation preceded CIP2A inhibition (Fig. S9D,F), whereas the ToBP1-related p-ATR and γ H2AX

501 induction occurred only after CIP2A protein inhibition (Fig. 6J and S9D,E,G-H).
502 Importantly, exogenous overexpression of CIP2A in MCF-10A cells, that were used to link
503 the results to G2/M arrest (Fig. 1E), and TopBP1 effects (Fig. 4G,H), abrogated SMAP-
504 elicited γ H2AX induction (Fig. 6K and S9I). CIP2A overexpression also shifted the SMAP
505 IC50 response in these cells (Fig. 6L). These results reveal that SMAPs have bi-phasic
506 therapeutic activity consisting of direct PP2A activation (14,16), followed by transcriptional
507 inhibition of *CIP2A* expression discovered here. SMAP-elicited CIP2A inhibition may thus
508 halt the growth of BLBC cells by both prolonging the PP2A reactivation effects, but also via
509 removing direct CIP2A-mediated direct effects on TopBP1 (Fig. 7).

510

511

512

Discussion

In this study, we provide comprehensive evidence that CIP2A overexpression can be a driver mechanism for BLBC initiation and malignant progression (Fig. 7). Consistent with the notion that even saturated genetic analysis of human breast cancers has failed to identify genetic BLBC driver, *CIP2A* gene sequence is not altered in BLBCs (<https://cancer.sanger.ac.uk/cosmic>). Instead, *CIP2A* expression is enhanced due to constitutive DNA-PK/CHK1 activity (48), TP53 inactivation (19), and EGFR pathway activation (20); which are all molecular hallmarks of BLBC (1,3)(Fig. 7). Transcriptional *CIP2A* induction early in DMBA-induced tumorigenesis is also fully supportive of its role in BLBC tumor initiation. Together these findings provide an explanation for high *CIP2A* expression in BLBC, whereas its newly discovered interaction with TopBP1 forms a molecular basis for its essential function in allowing malignant progression of DNA-damaged mammary epithelial cells towards BLBCs.

As opposed to previous assumptions that CIP2A is involved in the development of multiple human solid cancers (17), our results demonstrate selective involvement of CIP2A in initiation and progression of BLBCs both in human and mice. In addition to *in vivo* tumorigenesis results, in genetically defined cell culture models, only the *Brca1/Trp53* mutant basal-like cells were dependent on *Cip2a* for their colony growth. Also in human breast cancer samples, high CIP2A expression predicted for poor patient survival exclusively in BLBCs. The selectivity of CIP2A for BLBCs among the tumor types studied here, can be molecularly explained by the notion that CIP2A is able to coordinate BLBC hallmarks via promoting proliferative MYC and E2F1 activities, and at the same time blunting the G2/M checkpoint via its effects on the TopBP1/RAD51 complex (Fig. 7). In

addition to TopBP1, other highly CIP2A co-dependent DDR genes (Fig. 3A), not studied in this work, might confer its BLBC selectivity. One such candidate gene is POLQ (Fig. 3A, S4A,B), that is upregulated, and promotes genetic instability in BL-TNBC cells (49).

The functional homology of CIP2A with a number of critical DNA damage proteins (Fig. 3A), is likely one of the most important contributions of this work for the future studies. This is supported by the recent results demonstrating essentiality of CIP2A in different DDR-related genomic screens (40,50). Here we focused on validation of the novel interaction between nuclear CIP2A and TopBP1. Based on our results, TopBP1 can induce effective DDR in CIP2A deficient cells, whereas in CIP2A positive cells the TopBP1/RAD51 complex chromatin recruitment is dampened allowing for continued mitotic activity (Fig. 4K). This mechanism is fully in line with previous data related to TopBP1-mediated G2/M checkpoint regulation (5,7,9,11,43). As a notion, we validated the CIP2A function in TopBP1/RAD51 complex and in G2/M checkpoint activity in BRCA-proficient cells (Fig. 1E, 4E-J, S5B-E). Whether the same mechanism is behind essentiality of CIP2A for HRD cells, including BRCA-deficient BLBC cells, remains to be studied. Importantly, in our model the enhanced TopBP1/RAD51 chromatin recruitment is due to loss of a direct and PP2A-independent CIP2A-TopBP1 interaction (Fig. 7). On the other hand, CIP2A can protect proteins in the TopBP1-associated complex from PP2A-mediated dephosphorylation as indicated with NBN S432 phosphorylation data (38). In addition, similar to other models (19,33,35), CIP2A inhibited dephosphorylation of both MYC and E2F1 in BLBC cells. CIP2A expression is in turn driven by MYC and E2F1 (19,33), and we postulate that these positive feedback loops have critical role in maintaining high proliferative activity in BLBC. Collectively, we conclude that CIP2A-mediated BLBC

initiation and progression results from a mixture of its PP2A-dependent and -independent effects (Fig. 7).

In addition to identifying CIP2A as a driver candidate for BLBC, we demonstrate that SMAPs (14) function as transcriptional inhibitors of *CIP2A* expression. Our results reveal a model where SMAPs initially directly activate PP2A-B56 (14,16), and this followed by a prolonged PP2A activation due to transcriptional downregulation of *CIP2A*. Importantly, we were also able to demonstrate that CIP2A overexpression rescued the effects of SMAPs as assessed by both decreases in cell viability and γ H2AX regulation. However, it is important to note that we consider SMAPs as surrogate CIP2A inhibitors that also have acute effects not mediated by CIP2A inhibition, thereby explaining the anti-cancer effects of SMAPs noted in other cancer types (46,47). Importantly, we validated the therapeutic effects of three SMAPs across 15 different cell lines, including 6 individual patient-derived lines and a PDX model, together minimizing concerns related to compound specific effects, and known intratumoral heterogeneity of BLBC tumors.

Together these results credential CIP2A as a driver protein for one of the most aggressive human cancer types, BLBCs. We also discover a novel link between CIP2A and DDR via direct interaction with TopBP1. Generally, these results emphasize the importance in characterizing proteome level signaling dysregulation in the cancer subtypes for which genetic drivers are lacking.

584 **Acknowledgements**

585

586 We thank Taina Kalevo-Mattila for excellent technical assistance. Erica Nyman is thanked
 587 for help in IHC analysis. Professor Wojciech Niedzwiedz and Dr. Andrew Blackford are
 588 thanked for sharing research tools and protocols. We are very grateful to Ruth Keri Lab
 589 from Case Western Reserve University for sharing the PDX model. Dr. Michael Ohlmeyer
 590 (Atux Iskay LLC) is acknowledged for DBK-1154 and DBK-1160. Professor Johanna
 591 Ivaska and Dipanjan Chowdhury are acknowledged for their valuable comments to the
 592 data. We acknowledge Finnish Functional Genomics Center, Cell Imaging and Cytometry
 593 core facility, and Genome Editing Core at Turku Bioscience Centre, and Turku Centre for
 594 Disease Modeling (TCDM) all supported by Biocenter Finland, and/or ELIXIR Finland. The
 595 Central Laboratory Animal Facilities of University of Turku are acknowledged for help with
 596 the mouse models.

597 The project was funded by Academy of Finland (323096 for EP and 296801,
 598 314443 and 310561 for LE), Finnish Cancer Foundations (JW), Finnish Cultural
 599 Foundation (LE), Sigrid Juselius Foundation (JW, LE), Breast Cancer Now (JW, KW), and
 600 Governmental Research Funding for Turku University Hospital (TG). DCC is supported by
 601 the Fox Chase Cancer Center FCCC Core Grant NCI P30 CA006927. GN is supported by
 602 R01 CA181654, HL144741, CA240993, W81XWH-19-BCRP-BTA12 DOD and Rogel
 603 Cancer Gift Funds. JM is supported by Deutsche Forschungsgemeinschaft (DFG, German
 604 Research Foundation; PN(407869199)). AL was supported by Onco Institute, Svenska
 605 Kulturfonden, Orion Research Foundation, Relander Foundation, Inkeri and Mauri
 606 Vänskä's Foundation, Finnish Cultural Foundation's Varsinais-Suomi Regional Fund and
 607 by K. Albin Johanssons Stiftelse. SN was supported by the the University of Turku

608 Graduate School (UTUGS), Instrumentarium Science Foundation and Ida Montin
 609 Foundation.

610 **References:**

611

- 612 1. Denkert C, Liedtke C, Tutt A, von Minckwitz G. Molecular alterations in triple-
 613 negative breast cancer-the road to new treatment strategies. *Lancet*
 614 **2017**;389:2430-42
- 615 2. Rakha EA, Reis-Filho JS, Ellis IO. Basal-like breast cancer: a critical review. *J Clin*
 616 *Oncol* **2008**;26:2568-81
- 617 3. Duijf PHG, Nanayakkara D, Nones K, Srihari S, Kalimutho M, Khanna KK.
 618 Mechanisms of Genomic Instability in Breast Cancer. *Trends in molecular medicine*
 619 **2019**;25:595-611
- 620 4. Lehmann BD, Bauer JA, Chen X, Sanders ME, Chakravarthy AB, Shyr Y, *et al.*
 621 Identification of human triple-negative breast cancer subtypes and preclinical
 622 models for selection of targeted therapies. *J Clin Invest* **2011**;121:2750-67
- 623 5. Giunta S, Jackson SP. Give me a break, but not in mitosis: the mitotic DNA damage
 624 response marks DNA double-strand breaks with early signaling events. *Cell Cycle*
 625 **2011**;10:1215-21
- 626 6. Zheng XF, Kalev P, Chowdhury D. Emerging role of protein phosphatases changes
 627 the landscape of phospho-signaling in DNA damage response. *DNA repair*
 628 **2015**;32:58-65
- 629 7. Cotta-Ramusino C, McDonald ER, 3rd, Hurov K, Sowa ME, Harper JW, Elledge SJ.
 630 A DNA damage response screen identifies RHINO, a 9-1-1 and TopBP1 interacting
 631 protein required for ATR signaling. *Science* **2011**;332:1313-7

- 632 8. Sokka M, Parkkinen S, Pospiech H, Syvaoja JE. Function of TopBP1 in genome
 633 stability. *Subcell Biochem* **2010**;50:119-41
- 634 9. Kim WJ, Lee H, Park EJ, Park JK, Park SD. Gain- and loss-of-function of Rhp51, a
 635 Rad51 homolog in fission yeast, reveals dissimilarities in chromosome integrity.
 636 *Nucleic Acids Res* **2001**;29:1724-32
- 637 10. Liu Y, Smolka MB. TOPBP1 takes RADical command in recombinational DNA
 638 repair. *J Cell Biol* **2016**;212:263-6
- 639 11. Moudry P, Watanabe K, Wolanin KM, Bartkova J, Wassing IE, Watanabe S, *et al.*
 640 TOPBP1 regulates RAD51 phosphorylation and chromatin loading and determines
 641 PARP inhibitor sensitivity. *J Cell Biol* **2016**;212:281-8
- 642 12. Ogiwara H, Ui A, Onoda F, Tada S, Enomoto T, Seki M. Dpb11, the budding yeast
 643 homolog of TopBP1, functions with the checkpoint clamp in recombination repair.
 644 *Nucleic Acids Res* **2006**;34:3389-98
- 645 13. Chopra N, Tovey H, Pearson A, Cutts R, Toms C, Proszek P, *et al.* Homologous
 646 recombination DNA repair deficiency and PARP inhibition activity in primary triple
 647 negative breast cancer. *Nature communications* **2020**;11:2662
- 648 14. Leonard D, Huang W, Izadmehr S, O'Connor CM, Wiredja DD, Wang Z, *et al.*
 649 Selective PP2A Enhancement through Biased Heterotrimer Stabilization. *Cell*
 650 **2020**;181:688-701
- 651 15. Kauko O, Westermarck J. Non-genomic mechanisms of protein phosphatase 2A
 652 (PP2A) regulation in cancer. *Int J Biochem Cell Biol* **2018**;96:157-64
- 653 16. Vainonen JP, Momeny M, Westermarck J. Druggable cancer phosphatases.
 654 *Science translational medicine* **2021**;13
- 655 17. Khanna A, Pimanda JE. Clinical significance of Cancerous Inhibitor of Protein
 656 Phosphatase 2A (CIP2A) in human cancers. *Int J Cancer* **2015**

- 657 18. Côme C, Laine A, Chanrion M, Edgren H, Mattila E, Liu X, *et al.* CIP2A is
 658 associated with human breast cancer aggressivity. Clin Cancer Res **2009**;15:5092-
 659 100
- 660 19. Laine A, Sihto H, Come C, Rosenfeldt MT, Zwolinska A, Niemela M, *et al.*
 661 Senescence sensitivity of breast cancer cells is defined by positive feedback loop
 662 between CIP2A and E2F1. Cancer discovery **2013**;3:182-97
- 663 20. Khanna A, Okkeri J, Bilgen T, Tiirikka T, Vihinen M, Visakorpi T, *et al.* ETS1
 664 mediates MEK1/2-dependent overexpression of cancerous inhibitor of protein
 665 phosphatase 2A (CIP2A) in human cancer cells. PLoS ONE **2011**;6:e17979
- 666 21. Chao TT, Wang CY, Chen YL, Lai CC, Chang FY, Tsai YT, *et al.* Afatinib induces
 667 apoptosis in NSCLC without EGFR mutation through Elk-1-mediated suppression of
 668 CIP2A. Oncotarget **2015**;6:2164-79
- 669 22. Leonard D, Huang W, Izadmehr S, O'Connor CM, Wiredja DD, Wang Z, *et al.*
 670 Selective PP2A Enhancement through Biased Heterotrimer Stabilization. Cell
 671 **2020**;181:688-701 e16
- 672 23. Kim S, Roopra A, Alexander CM. A phenotypic mouse model of basaloid breast
 673 tumors. PLoS One **2012**;7:e30979
- 674 24. Liu X, Holstege H, van der Gulden H, Treur-Mulder M, Zevenhoven J, Velds A, *et*
 675 *al.* Somatic loss of BRCA1 and p53 in mice induces mammary tumors with features
 676 of human BRCA1-mutated basal-like breast cancer. Proc Natl Acad Sci U S A
 677 **2007**;104:12111-6
- 678 25. Derksen PW, Liu X, Saridin F, van der Gulden H, Zevenhoven J, Evers B, *et al.*
 679 Somatic inactivation of E-cadherin and p53 in mice leads to metastatic lobular
 680 mammary carcinoma through induction of anoikis resistance and angiogenesis.
 681 Cancer Cell **2006**;10:437-49

- 682 26. Wellenstein MD, Coffelt SB, Duits DEM, van Miltenburg MH, Slagter M, de Rink I, *et al.* Loss of p53 triggers WNT-dependent systemic inflammation to drive breast
 683 cancer metastasis. *Nature* **2019**;572:538-42
- 685 27. Metzger E, Stepputtis SS, Strietz J, Preca BT, Urban S, Willmann D, *et al.* KDM4
 686 Inhibition Targets Breast Cancer Stem-like Cells. *Cancer Res* **2017**;77:5900-12
- 687 28. Ventelä S, Côme C, Mäkelä JA, Hobbs RM, Mannermaa L, Kallajoki M, *et al.* CIP2A
 688 promotes proliferation of spermatogonial progenitor cells and spermatogenesis in
 689 mice. *PLoS ONE* **2012**;7:e33209
- 690 29. Kucab JE, Zou X, Morganella S, Joel M, Nanda AS, Nagy E, *et al.* A Compendium
 691 of Mutational Signatures of Environmental Agents. *Cell* **2019**;177:821-36 e16
- 692 30. Connolly DC, Bao R, Nikitin AY, Stephens KC, Poole TW, Hua X, *et al.* Female
 693 mice chimeric for expression of the simian virus 40 TAg under control of the MISIR
 694 promoter develop epithelial ovarian cancer. *Cancer Res* **2003**;63:1389-97
- 695 31. Blomen VA, Majek P, Jae LT, Bigenzahn JW, Nieuwenhuis J, Staring J, *et al.* Gene
 696 essentiality and synthetic lethality in haploid human cells. *Science* **2015**;350:1092-6
- 697 32. Abba MC, Zhong Y, Lee J, Kil H, Lu Y, Takata Y, *et al.* DMBA induced mouse
 698 mammary tumors display high incidence of activating Pik3caH1047 and loss of
 699 function Pten mutations. *Oncotarget* **2016**;7:64289-99
- 700 33. Khanna A, Böckelman C, Hemmes A, Junttila MR, Wiksten JP, Lundin M, *et al.*
 701 MYC-dependent regulation and prognostic role of CIP2A in gastric cancer. *J Natl*
 702 *Cancer Inst* **2009**;101:793-805
- 703 34. Myant K, Qiao X, Halonen T, Come C, Laine A, Janghorban M, *et al.* Serine 62-
 704 Phosphorylated MYC Associates with Nuclear Lamins and Its Regulation by CIP2A
 705 Is Essential for Regenerative Proliferation. *Cell reports* **2015**;12:1019-31

- 706 35. Janghorban M, Farrell AS, Allen-Petersen BL, Pelz C, Daniel CJ, Oddo J, *et al.*
 707 Targeting c-MYC by antagonizing PP2A inhibitors in breast cancer. *Proc Natl Acad*
 708 *Sci U S A* **2014**;111:9157-62
- 709 36. Niemela M, Kauko O, Sihto H, Mpindi JP, Nicorici D, Pernila P, *et al.* CIP2A
 710 signature reveals the MYC dependency of CIP2A-regulated phenotypes and its
 711 clinical association with breast cancer subtypes. *Oncogene* **2012**;31:4266-78
- 712 37. Oskarsson T, Essers MA, Dubois N, Offner S, Dubey C, Roger C, *et al.* Skin
 713 epidermis lacking the c-Myc gene is resistant to Ras-driven tumorigenesis but can
 714 reacquire sensitivity upon additional loss of the p21Cip1 gene. *Genes Dev*
 715 **2006**;20:2024-9
- 716 38. Kauko O, Imanishi SY, Kuleskiy E, Yetukuri L, Laajala TD, Sharma M, *et al.*
 717 Phosphoproteome and drug-response effects mediated by the three protein
 718 phosphatase 2A inhibitor proteins CIP2A, SET, and PME-1. *J Biol Chem*
 719 **2020**;295:4194-211
- 720 39. Wohlbold L, Merrick KA, De S, Amat R, Kim JH, Larochelle S, *et al.* Chemical
 721 genetics reveals a specific requirement for Cdk2 activity in the DNA damage
 722 response and identifies Nbs1 as a Cdk2 substrate in human cells. *PLoS genetics*
 723 **2012**;8:e1002935
- 724 40. DeWeirdt PC, Sangree AK, Hanna RE, Sanson KR, Hegde M, Strand C, *et al.*
 725 Genetic screens in isogenic mammalian cell lines without single cell cloning. *Nature*
 726 *communications* **2020**;11:752
- 727 41. Liu S, Bekker-Jensen S, Mailand N, Lukas C, Bartek J, Lukas J. Claspin operates
 728 downstream of TopBP1 to direct ATR signaling towards Chk1 activation. *Mol Cell*
 729 *Biol* **2006**;26:6056-64

- 730 42. Chowdhury D, Keogh MC, Ishii H, Peterson CL, Buratowski S, Lieberman J.
 731 gamma-H2AX dephosphorylation by protein phosphatase 2A facilitates DNA
 732 double-strand break repair. *Mol Cell* **2005**;20:801-9
- 733 43. Yamane K, Chen J, Kinsella TJ. Both DNA topoisomerase II-binding protein 1 and
 734 BRCA1 regulate the G2-M cell cycle checkpoint. *Cancer Res* **2003**;63:3049-53
- 735 44. Wang J, Okkeri J, Pavic K, Wang Z, Kauko O, Halonen T, *et al.* Oncoprotein CIP2A
 736 is stabilized via interaction with tumor suppressor PP2A/B56. *EMBO reports*
 737 **2017**;18:437-50
- 738 45. Sangodkar J, Perl A, Tohme R, Kiselar J, Kastrinsky DB, Zaware N, *et al.* Activation
 739 of tumor suppressor protein PP2A inhibits KRAS-driven tumor growth. *J Clin Invest*
 740 **2017**;127:2081-90
- 741 46. Kauko O, O'Connor CM, Kuleskiy E, Sangodkar J, Aakula A, Izadmehr S, *et al.*
 742 PP2A inhibition is a druggable MEK inhibitor resistance mechanism in KRAS-
 743 mutant lung cancer cells. *Science translational medicine* **2018**;10
- 744 47. Farrington CC, Yuan E, Mazhar S, Izadmehr S, Hurst L, Allen-Petersen BL, *et al.*
 745 Protein phosphatase 2A activation as a therapeutic strategy for managing MYC-
 746 driven cancers. *J Biol Chem* **2020**;295:757-70
- 747 48. Khanna A, Kauko O, Böckelman C, Laine A, Schreck I, Partanen JI, *et al.* Chk1
 748 Targeting Reactivates PP2A Tumor Suppressor Activity in Cancer Cells. *Cancer*
 749 *Research* **2013**;73:6757-69
- 750 49. Prodhomme MK, Pommier RM, Franchet C, Fauvet F, Bergoglio V, Brousset P, *et*
 751 *al.* EMT transcription factor ZEB1 represses the mutagenic POLtheta-mediated
 752 end-joining pathway in breast cancers. *Cancer Research* **2020**;81:1595-606
- 753 50. Hustedt N, Alvarez-Quilon A, McEwan A, Yuan JY, Cho T, Koob L, *et al.* A
 754 consensus set of genetic vulnerabilities to ATR inhibition. *Open Biol* **2019**;9:190156

Figure legends:

Figure 1. *Cip2a* knockout mice are selectively resistant to DMBA-induced mammary tumorigenesis. **A**, DMBA was orally administered to wild type (*WT*) and *Cip2a*^{-/-} mice once a week for 6 consecutive weeks after which mice were monitored for signs of spontaneous tumor formation. **B**, Number of genetic variants in exons of the expressed genes in non-treated (control) and DMBA-treated *WT* (n=3) and *Cip2a*^{-/-} (n=3) mouse mammary glands. P-value by Wilcoxon test. **C**, Incidences of tumor formation in different tissues in sacrificed DMBA-administered *WT* (n=18) and *Cip2a*^{-/-} (n=14) mice. P-values between *WT* and *Cip2a*^{-/-} groups calculated by Fisher's exact test. **D**, Incidence of mammary tumors in *WT* (n=18) and *Cip2a*^{-/-} (n=14) mice after starting administration of DMBA. P-value by log-rank test. **E**, Mitotic index analysis of MCF10A cells transfected with the indicated siRNAs. Cells were treated with 10Gy radiation dose and Nocodazole (100 ng/ml) block 1 hour after IR for 18 hours. Mitotic cells were stained using phospho-histone H3 at Ser10. Scale bar: 100µm. Bar graph shows % of H3pS10 positive nuclei from three replicates, expressed as mean ± SD. **F**, Heat map of fraction of gene-trap insertions in the sense orientation compared to the total (sense and anti- sense) insertions in untreated HAP1 cells and HAP1 cells treated with successive low doses of IR (5x 1Gy). Color coding indicates essentiality of the indicated PP2A inhibitor protein for cell survival.

Figure 2: *Cip2a* drives initiation of mouse BLBC-like tumors **A**, qRT-PCR analysis of *Cip2a* mRNA expression normalized to *Actb* and *Gapdh* from *WT* and *Cip2a*^{-/-} non-treated

780 (Ctrl) and DMBA-administered mouse non-tumorigenic mammary glands (MG), and from
 781 WT DMBA-induced mammary tumors. Shown is mean \pm SD of 10 *WT* and 9 *Cip2a*^{-/-} non-
 782 treated mammary glands (Ctrl MG), 3 *WT*, and 3 *Cip2a*^{-/-} mammary glands from DMBA-
 783 administered mice, and 16 mammary tumors. P-values calculated by Mann-Whitney test.
 784 **B**, Representative images of immunohistochemical staining of Keratin-14 (K14), Keratin-8
 785 (K8), CIP2A, Ki67 and MYC proteins and hematoxylin and eosin (HE) from DMBA-induced
 786 mammary tumors from *WT* mice. Scale bar: 50 μ M **C**, Semiquantitative analysis of receptor
 787 status from 10 WT tumors. **D**, Top five enriched hallmark gene sets based on differentially
 788 regulated genes in non-tumorigenic *Cip2a* KO mouse mammary glands treated with six
 789 doses of DMBA.

790

791 **Figure 3: Co-dependence analysis reveals functional association of CIP2A with**
 792 **critical DNA damage response proteins** **A**, Top 10 co-dependencies with *CIP2A* across
 793 739 cell lines genome-wide from CRISPR Avena screen. *CIP2A*'s own co-dependency
 794 rank for the top 10 genes is also listed. Data extracted from DepMap portal (Avena
 795 2020Q1). **B**, Genome-widely, *CIP2A* is the closest functional homologue to *RHNO1* and
 796 *TOPBP1*. **C**, STRING functional protein association network analysis of CIP2A co-
 797 dependent proteins from (A). By using the highest data confidence score (0.9), except for
 798 APEX2, DSCC1 and CIP2A, the other proteins form highly connected protein network.
 799 NBN phosphorylation indicated by red dot was found to be regulated by CIP2A based on
 800 (38). **D**, Top 10 Reactome pathways associated with genes from (A). **E**, Correlation
 801 between *CIP2A* and *TOPBP1* mRNA expression across 1156 cell lines from Cancer Cell
 802 Line Encyclopedia. **F**, Pair-wise correlation of dependence of either BLBC or HGSOC cell
 803 lines of the indicated genes from DepMap portal (Avena 2020Q1). The values for BLBC

804 and HGSOC indicates correlation (max. 1) in dependence of the cells for the genes in the
 805 gene pair; the higher number indicating for higher similarity in the dependence. The color-
 806 coded numbers indicate the difference in the co-dependence between BLBC and HGSOC
 807 cells for the indicated gene pair.

808

809 **Figure 4: CIP2A is an interacting partner of TopBP1 and promotes mitotic**
 810 **progression of DNA damaged cells. A,** Schematic presentation of breast cancer cell line
 811 cDNA fragments coding for TopBP1 domains that interact with full length CIP2A in a yeast
 812 two-hybrid assay. Numbers in the TopBP1 drawing refer to BRCT domains 1-8; AAD, ATR
 813 activation domain. Analysis of the minimal common overlapping region between the
 814 TopBP1 fragments interacting with CIP2A reveal the TopBP1 aa. 829-853 as a candidate
 815 CIP2A interaction domain. **B,** Co-immunoprecipitation of endogenous CIP2A and γ H2AX
 816 in HEK293 cells transiently overexpressing GFP or full length TopBP1-GFP as indicated.
 817 Input 5% of total IP. **C,** Co-immunoprecipitation of CIP2A in HEK293 cells transiently
 818 overexpressing V5-tagged CIP2A and GFP-tagged Empty vector (EV) or TopBP1
 819 truncated mutants T0, T1, T2, T3 as indicated in (D). Input 5% of total IP. **D,** Schematic
 820 representation of TopBP1 mutants used in (B,C) Relative interaction efficiencies are
 821 estimated from the experiment where all indicated mutants were included. **E,** Immortalized
 822 MCF10A cells transfected with non-targeting (SCR) or *CIP2A* siRNAs for 48hrs.
 823 Immunoblot of whole cell extracts (WCEs) probed for pATR, total ATR and CIP2A. Vinculin
 824 was used as a loading control. Relative quantifications of pATR/ATR and CIP2A plotted as
 825 Mean \pm SD from five replicates. **F,** MDA-MB-231 cells transfected with non-targeting (SCR)
 826 and *CIP2A* targeting siRNAs for 72 hrs and overexpressing TopBP1 mutants T0 and T1 as
 827 indicated for 48 hours. Immunoblot of WCEs probed for pATR, γ H2AX and CIP2A. Actin

was used as a loading control. Relative quantifications of γ H2AX plotted as Mean \pm SD from two replicates. **G**, IR-induced TopBP1 foci formation in MCF10A cells transfected with *SCR* or *CIP2A* siRNA as indicated for 48 hrs. Cells were treated with 5Gy radiation for 1 hour and stained for CIP2A or TopBP1. **H**, Quantifications of the nuclear foci from (G) expressed as mean \pm SD from representative experiment of three experiments with similar results **I**, IR-induced RAD51 foci formation in mouse mammary epithelial cells (MMECs) isolated from *WT* and *Cip2a*^{-/-} mice cultured *in-vitro* for 48 hrs, treated with 5Gy radiation for 2 hours. **J**, Quantifications of the foci in expressed as mean \pm SD of representative experiment. **G-J**, Images were taken at 63X on 3i spinning disk confocal and at least 150 cells quantified per each condition using speckle counter pipeline on Cell Profiler. Scale bar: 10 μ M. **E-J**, All statistical analyses were conducted with Welch's Student t-test for unequal variances, *p<0.05, ** p<0.01 **K**, Schematic presentation of the role of CIP2A in directly inhibiting TopBP1/RAD51-elicited G2/M checkpoint activation in non-transformed mammary epithelial cells.

Figure 5: CIP2A is essential for survival of TP53/BRCA-mutant BLBC cells and drives proliferative signaling **A**, Expression of *CIP2A* mRNA in indicated molecular breast cancer subtypes. Data derived from TCGA. P-values by unpaired t-test. **B**, Disease-free survival of *CIP2A* high (n=15) and *CIP2A* low (n=45) expressing basal-like TNBC patients in GSE21653 cohort. **C**, Disease-free survival of *CIP2A* high (n=45) and *CIP2A* low (n=132) expressing non-basal-like (HER2+, luminal A, luminal B and normal-like) breast cancer patients in GSE21653 cohort. **D**, Overall survival of *CIP2A* high (n=12) and *CIP2A* low (n=51) basal-like TNBC patients in FinHer cohort. **E**, Overall survival of *CIP2A* high (n=17) and *CIP2A* low (n=47) non-basal like TNBC patients based IHC analysis from FinHer cohort. **B-E**, P-values calculated by log-rank test. **F**, *CIP2A*

dependence of breast cancer cell lines with CERES score < -0.4 from DepMap portal (Avana 2020Q1). Lower CERES scores indicate that the cell line is more dependent on *CIP2A*. Color coding indicates the breast cancer subtype of the cell line based on PAM50 classification. **G**, Colony growth assays conducted on mammary tumor cell lines isolated from basal-type (*KB1P#1* and *KB1P#2*: *Brca1* and *Trp53* mutant) and invasive lobular carcinoma (ILC)-type (*KEP#1* and *KEP#2*: *E-Cadherin* and *Trp53* mutant) mouse models; *Cip2a* was knocked out using CRISPR/Cas9 using 2 unique gRNAs. Western blots from the same samples probed for CIP2A below. Shown are representative images of at least 2 independent biological repeats for each cell line. **H**, Summary of *CIP2A*-dependence on colony growth of indicated *TP53*-mutant TNBC cell lines transfected with Mock, non-targeting siRNA (*siSCR*), or three unique *CIP2A* targeting siRNAs (*siCIP2A* #1, #2, #3). Colony areas were quantified and normalized to *siSCR*. **I**, Gene Set Enrichment Analysis (GSEA) conducted on differentially expressed genes obtained from RNA-seq of HCC38 cells depleted with 3 unique *CIP2A* siRNAs. **J**, HCC38 cells transfected with *SCR* or *CIP2A* siRNAs for 72 hrs and immunoblotted for indicated protein.

868

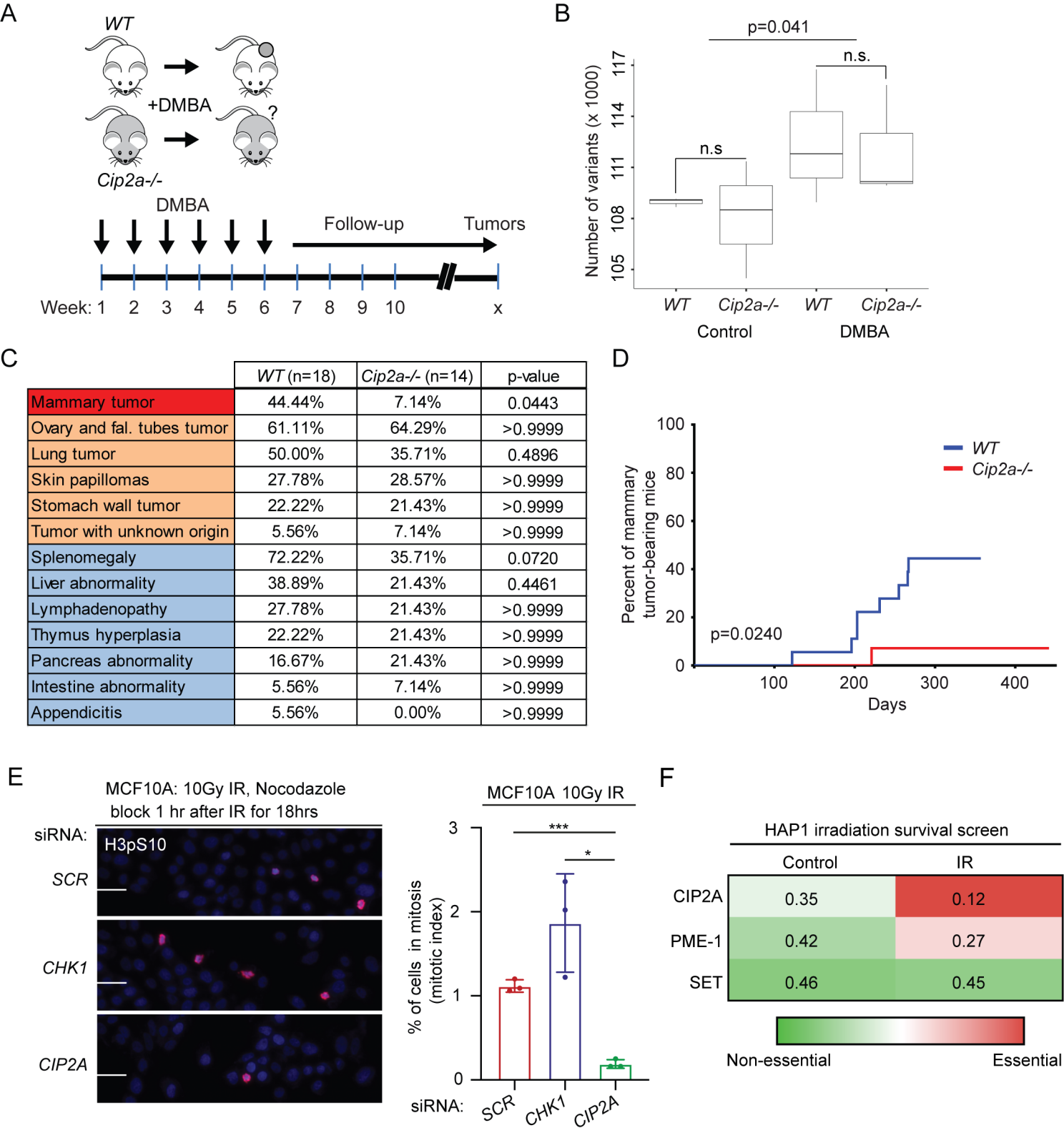
Figure 6: CIP2A targeting by SMAPs as potential BLBC therapy **A**, SMAP (DBK-1154) sensitivity profiles of eight BL-TNBC cell lines. Cell viabilities were measured using CellTiterGlo Luminescence Assay after 24 hrs of drug treatment. EC50s are listed in parentheses. **B**, Screening of patient-derived BLBC stem cell like cells for chemotherapy and SMAP responses. Heatmap indicates the drug sensitivity scores (DSS) of these cells across standard chemotherapeutics and three SMAPs DBK-1154, DT-061, NZ-1160). Higher DSS value indicates higher sensitivity. **C**, Tumor growth of an orthotopic patient derived xenograft model of basal triple negative breast cancer treated with DMA or 5mpk BID SMAP DT-061 for 43 days. Respective quantifications are represented as mean \pm SD.

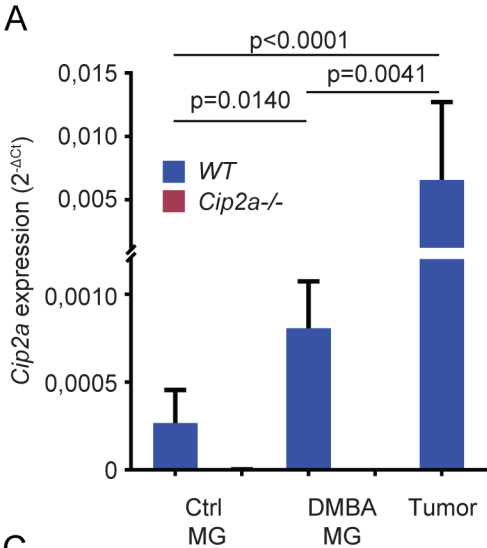
878 **D,E**, CIP2A western blots from MDA-MB-468 (D) and patient-derived stem cell-like cells,
 879 BCSC1 (E) on treatment with indicated SMAPs for 24h. DT-061 and DBK-1154
 880 concentration 20 μ M. **F**, Kinetics of *CIP2A* mRNA expression from MDA-MB-468 cells after
 881 treatment with 20uM of DT-061. n=3 expressed as mean \pm SD. **G**, Kinetics of pT202/Y204-
 882 ERK, CIP2A and pS62-MYC from MDA-MB-468 cell line treated with SMAP DT-061
 883 (20uM) for indicated time points. Representative western blot data shown in Fig. S8H. n=3
 884 expressed as mean \pm SD. **H**, Quantification of Western blots of MDA-MB-468 cell line
 885 treated with 20 μ M SMAP DT-061 for 24 hrs and probed for γ H2AX, represented as mean
 886 \pm SD from n=3 replicates normalized to the untreated controls. **I**, Quantification of western
 887 blots from MDA-MB-468 cell line treated with 20uM of DT-061 for 24hrs, displayed in Fig.
 888 S9A. Data expressed as mean \pm SD from n=3 replicates normalized to the untreated
 889 controls. **J**, Time course of CIP2A and γ H2AX protein expression in MDA-MB-468 treated
 890 with DT-061 (20 μ M) for indicated time periods. Western blot data are shown in Fig. S8F
 891 and S9B. **K**, CIP2A overexpression in MCF10A cell line rescues the SMAP-elicited γ H2AX
 892 activation. Western blots of parental and CIP2A OE MCF10A cells treated with SMAP
 893 DBK-1154 for 24hrs and probed for γ H2AX. GAPDH is used as loading control; γ H2AX
 894 quantifications from n=4 replicates displayed below. **L**, Dose response curve of control and
 895 CIP2A OE stable cell line (CIP2A OE) MCF10A cells on treatment with concentration
 896 series of DBK-1154 for 24 hours. IC50 values indicated in parenthesis. **A-L**, p-values
 897 calculated using unpaired t-test, *P<0.05, **P<0.01, *** P<0.001, ****P<0.0001.

898

899 **Figure 7. Schematic presentation of the role for CIP2A in coordinating BLBC**
 900 **molecular hallmarks.** The capacity of CIP2A to co-ordinately regulate G2/M checkpoint,
 901 and proliferative signaling by MYC and E2F1, provides a molecular basis for its role as
 902 BLBC driver. Black arrows indicate known mechanisms implicated in BLBC that either

903 regulate CIP2A expression and/or promote BLBC progression. Green arrows indicate
 904 PP2A inhibition-dependent mechanisms by which CIP2A increase proliferation capacity of
 905 BLBC cells. The PP2A-dependence of these mechanisms has been demonstrated
 906 previously (19,36). The orange block arrow indicates direct binding of CIP2A to TopBP1
 907 and inhibition of TopBP1-mediated checkpoint activity in response to DSB in premalignant
 908 mammary epithelial cells. Green block arrow indicates potential PP2A-dependent
 909 regulation of NBN phosphorylation. Collectively, CIP2A both responds to hallmarks of
 910 BLBCs (p53 inhibition, EGFR activity and HR defects) and co-ordinately controls the
 911 essential functional hallmarks; G2/M checkpoint and high proliferation activity. The
 912 relationship between CIP2A and BLBC hallmarks is also a plausible explanation for the
 913 selective role for CIP2A in BLBC as compared to other cancer types.

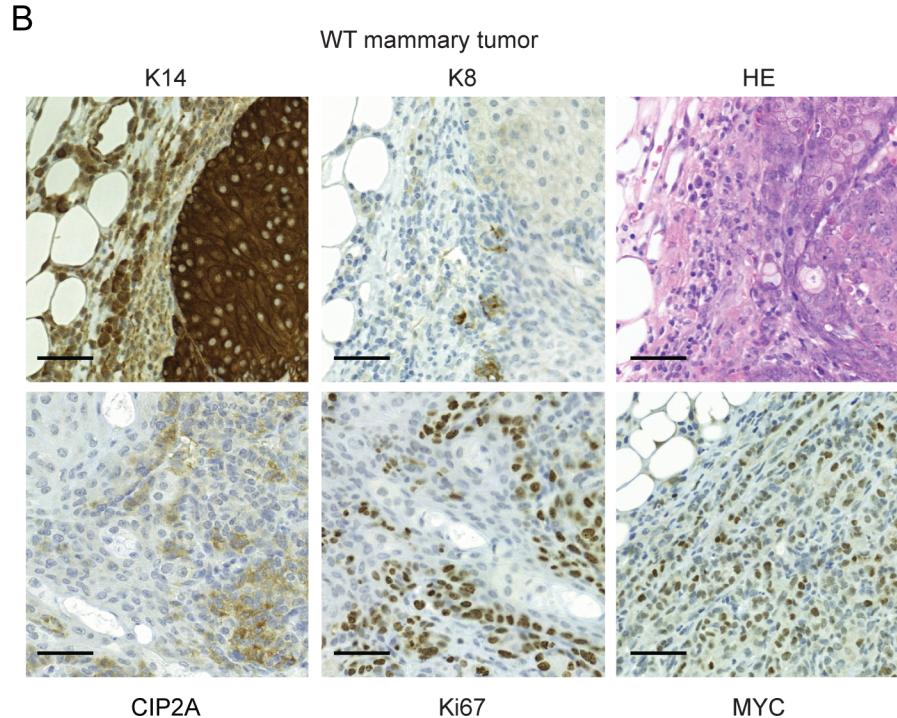




C

Receptor status of WT mammary tumors

Tumor	ER	PR	HER2
#1	-	-/+	-
#2	-	-	-
#3	-/+	+	-
#4	-	-/+	-
#5	-	-	-
#6	+	+	-
#7	+	+	-
#8	-	+	-
#9	-	-	-
#10	-	-	-



D

RNASeq: non tumorigenic *Cip2a* KO vs WT mouse MGs

Top 5 Hallmark gene sets enriched in genes downregulated in *Cip2a* KO

GENE SET NAME	NES	FDR q-value
HALLMARK_OXIDATIVE_PHOSPHORYLATION	-3.071	0
HALLMARK_E2F_TARGETS	-2.928	0
HALLMARK_MYC_TARGETS_V1	-2.840	0
HALLMARK_G2M_CHECKPOINT	-2.605	0
HALLMARK_MYC_TARGETS_V2	-2.527	0

A

CRISPR Avana 2020 Q1 data from Depmap

CIP2A co-dependent genes		
Gene	Dependency correlation	CIP2A's association rank with the gene
1. <i>RHNO1</i>	0.486	1
2. <i>H2AX</i>	0.402	3
3. <i>TOPBP1</i>	0.392	1
4. <i>MDC1</i>	0.339	4
5. <i>POLQ</i>	0.327	1
6. <i>NBN</i>	0.315	1
7. <i>XRCC1</i>	0.302	2
8. <i>APEX2</i>	0.295	2
9. <i>PARP1</i>	0.294	1
10. <i>DSCC1</i>	0.280	7

B

RHNO1 co-dependent genes

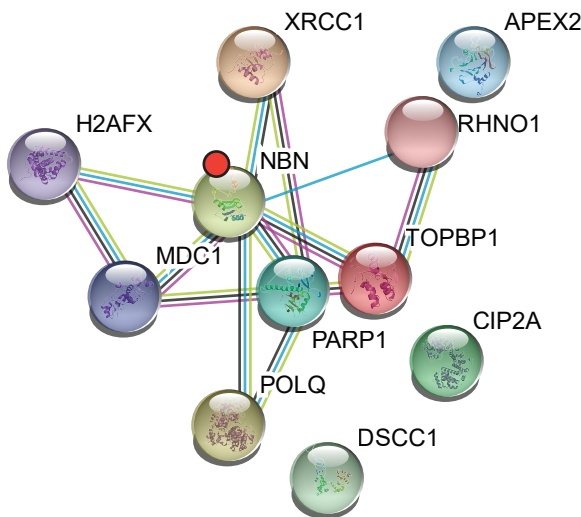
Gene	Dependency correlation
1. <i>CIP2A</i>	0.49
2. <i>H2AX</i>	0.34
3. <i>RNF168</i>	0.32
4. <i>TOPBP1</i>	0.31
5. <i>MDC1</i>	0.31

TOPBP1 co-dependent genes

Gene	Dependency correlation
1. <i>CIP2A</i>	0.39
2. <i>RAD17</i>	0.31
3. <i>RHNO1</i>	0.31
4. <i>MDC1</i>	0.27
5. <i>ATR</i>	0.27

C

STRING analysis; highest confidence score (0.9)



● CIP2A-regulated phosphosite (FDR < 0.05)

D

Reactome pathways associated with *CIP2A* co-dependent genes

Pathway	Description	FDR
HSA-5693538	Homology Directed Repair	4.44E-14
HSA-5685939	HDR through MMEJ (alt-NHEJ)	1.47E-09
HSA-69473	G2/M DNA damage checkpoint	1.20E-08
HSA-5693607	Processing of DNA double-strand break ends	1.20E-08
HSA-5685938	HDR through Single Strand Annealing (SSA)	1.30E-05
HSA-5693616	Presynaptic phase of homologous DNA pairing and strand exchange	1.38E-05
HSA-5693571	Nonhomologous End-Joining (NHEJ)	2.86E-05
HSA-5693565	Recruitment and ATM-mediated phosphorylation of repair and signaling proteins at DNA double strand breaks	3.82E-05
HSA-212436	Generic Transcription Pathway	7.47E-05
HSA-6804756	Regulation of TP53 Activity through Phosphorylation	1.00E-04

F

	BLBC	HGSOC	BLBC-HGSOC
<i>CIP2A</i> vs. <i>TOPBP1</i>	0,263	-0,141	0,404
<i>CIP2A</i> vs. <i>NBN</i>	0,819	0,510	0,309
<i>CIP2A</i> vs. <i>POLQ</i>	0,507	0,520	-0,013
<i>CIP2A</i> vs. <i>PARP1</i>	0,378	0,422	-0,043
<i>CIP2A</i> vs. <i>RHNO1</i>	0,195	0,699	-0,504

BLBC co-dependent

HGSOC co-dependent

E

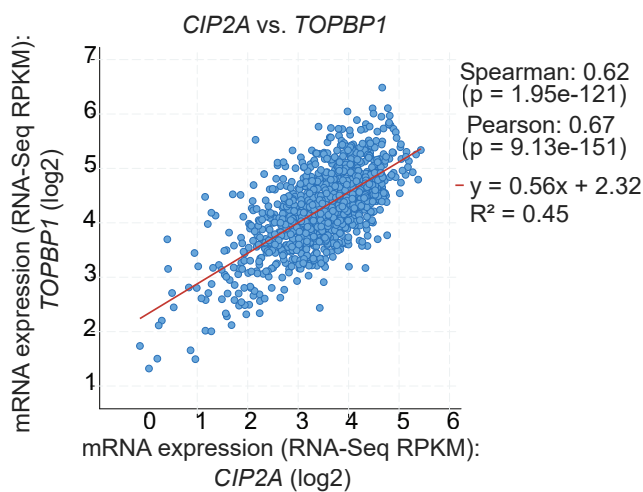
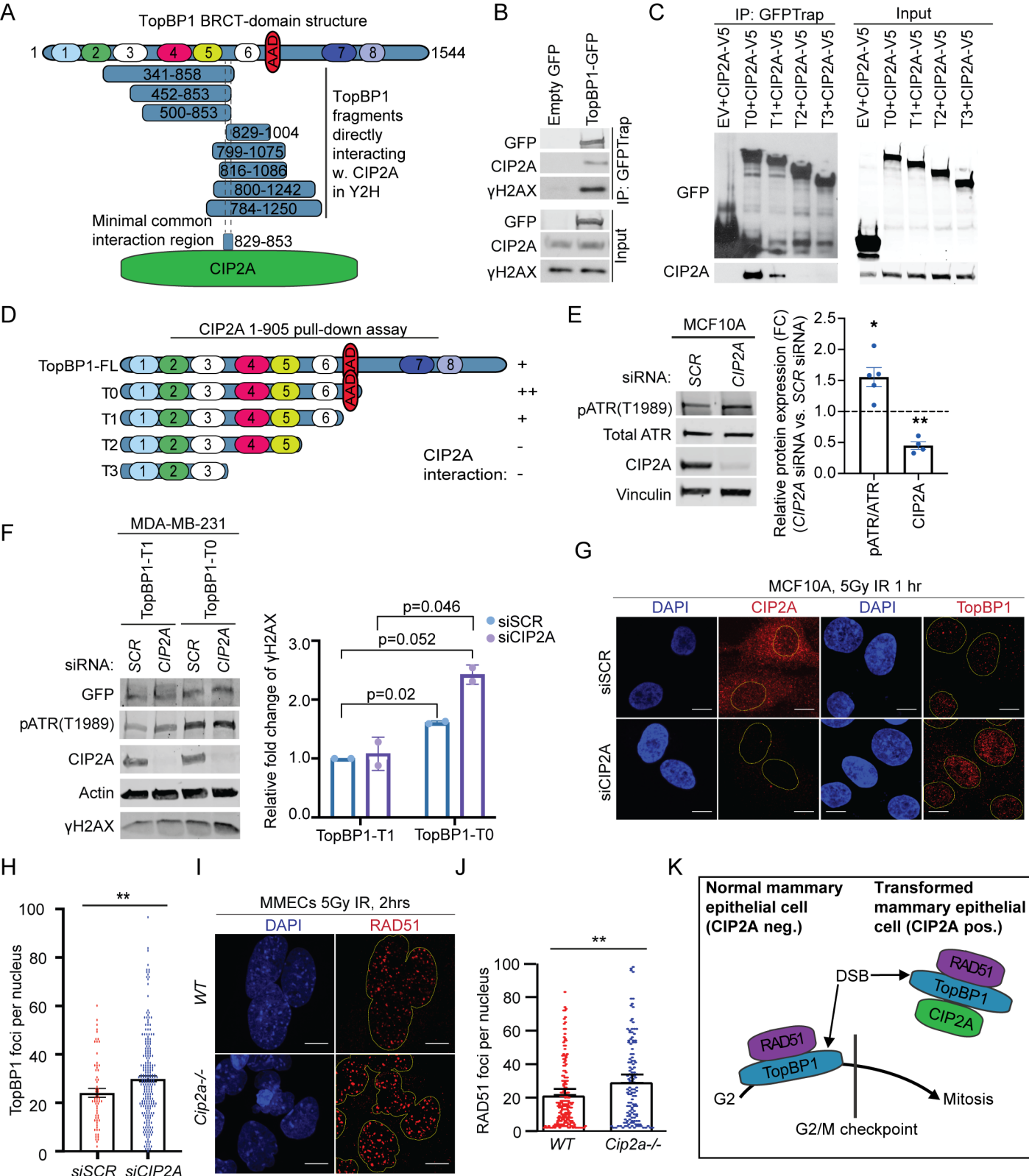
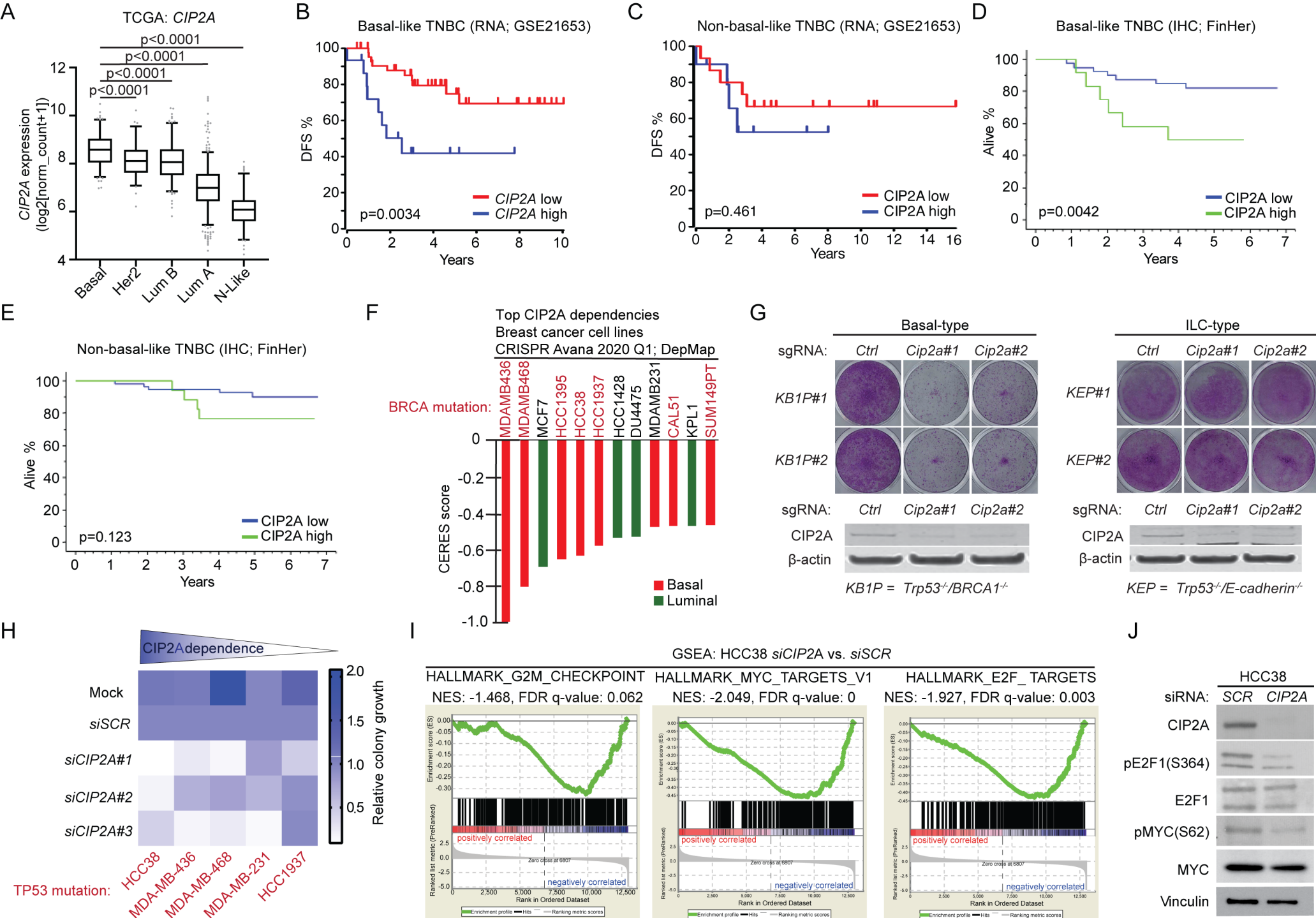
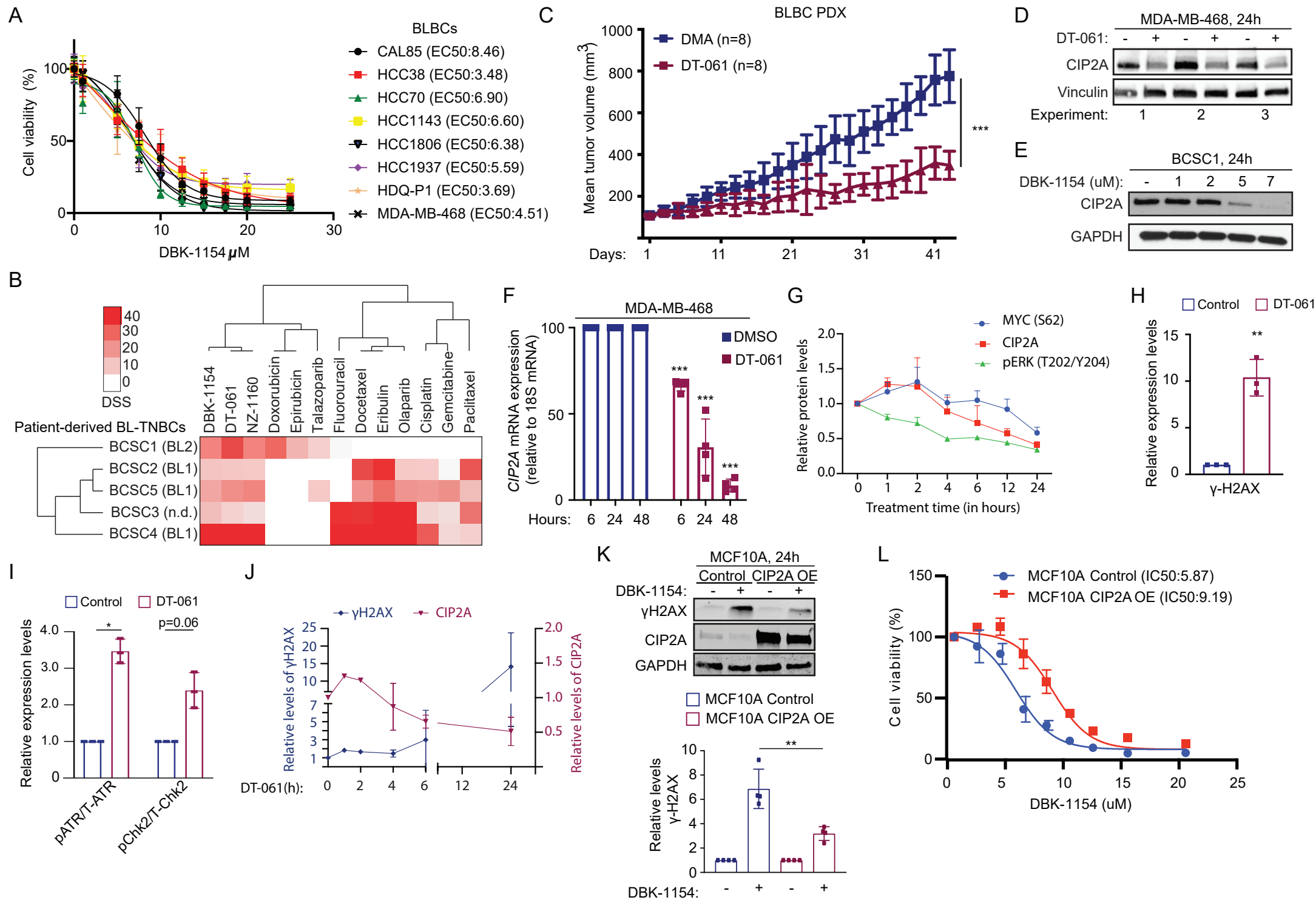


Figure 3







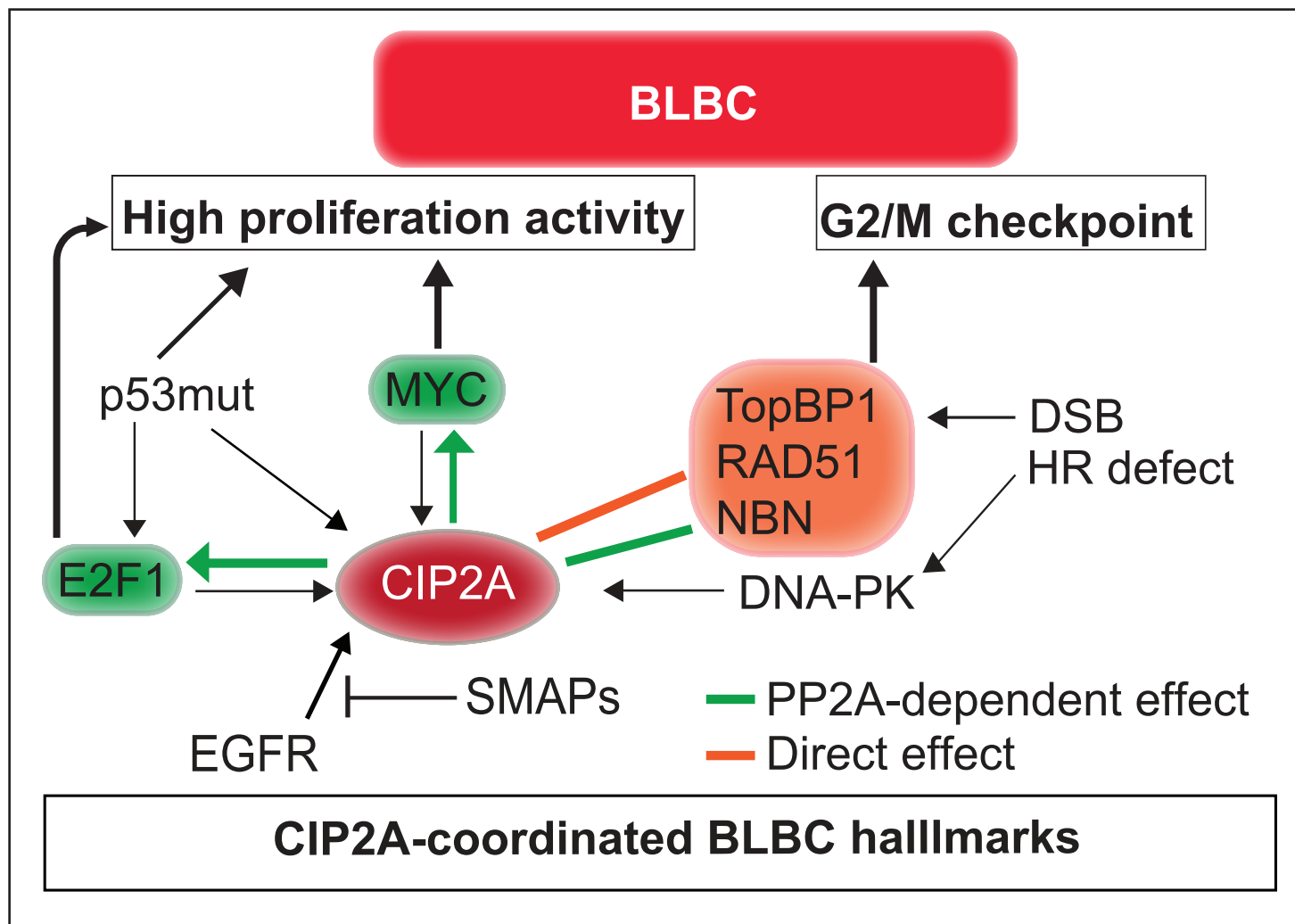


Figure 7

Cancer Research

The Journal of Cancer Research (1916–1930) | The American Journal of Cancer (1931–1940)

CIP2A interacts with TopBP1 and drives basal-like breast cancer tumorigenesis

Anni Laine, Srikar G. Nagelli, Caroline Farrington, et al.

Cancer Res Published OnlineFirst June 18, 2021.

Updated version	Access the most recent version of this article at: doi: 10.1158/0008-5472.CAN-20-3651
Supplementary Material	Access the most recent supplemental material at: http://cancerres.aacrjournals.org/content/suppl/2021/06/18/0008-5472.CAN-20-3651.DC1
Author Manuscript	Author manuscripts have been peer reviewed and accepted for publication but have not yet been edited.

E-mail alerts	Sign up to receive free email-alerts related to this article or journal.
Reprints and Subscriptions	To order reprints of this article or to subscribe to the journal, contact the AACR Publications Department at pubs@aacr.org .
Permissions	To request permission to re-use all or part of this article, use this link http://cancerres.aacrjournals.org/content/early/2021/06/18/0008-5472.CAN-20-3651 . Click on "Request Permissions" which will take you to the Copyright Clearance Center's (CCC) Rightslink site.